



# CHORUS

This is the accepted manuscript made available via CHORUS. The article has been published as:

## Concurrent probing of electron-lattice dephasing induced by photoexcitation in 1T-TaSeTe using ultrafast electron diffraction

Jun Li, Junjie Li, Kai Sun, Lijun Wu, Renkai Li, Jie Yang, Xiaozhe Shen, Xijie Wang, Huixia Luo, Robert J. Cava, Ian K. Robinson, Xilian Jin, Weiguo Yin, Yimei Zhu, and Jing Tao

Phys. Rev. B **101**, 100304 — Published 31 March 2020

DOI: [10.1103/PhysRevB.101.100304](https://doi.org/10.1103/PhysRevB.101.100304)

# Concurrent probing of electron-lattice dephasing induced by photoexcitation in 1T-TaSeTe using ultrafast electron diffraction

Jun Li<sup>1</sup>, Junjie Li<sup>1</sup>, Kai Sun<sup>2</sup>, Lijun Wu<sup>1</sup>, Renkai Li<sup>3</sup>, Jie Yang<sup>3</sup>, Xiaozhe Shen<sup>3</sup>, Xijie Wang<sup>3</sup>, Huixia Luo<sup>4</sup>, Robert J. Cava<sup>4</sup>, Ian K. Robinson<sup>1,5</sup>, Xilian Jin<sup>1,6</sup>, Weiguo Yin<sup>1</sup>, Yimei Zhu<sup>1</sup>, Jing Tao<sup>1,\*</sup>

<sup>1</sup>Condensed Matter Physics & Materials Science Department, Brookhaven National Laboratory, Upton, NY 11973, USA

<sup>2</sup>Department of Physics, University of Michigan, Ann Arbor, MI 48109, USA

<sup>3</sup>SLAC National Accelerator Laboratory, Menlo Park, CA, USA.

<sup>4</sup>Department of Chemistry, Princeton University, Princeton, NJ 08544, USA

<sup>5</sup>London Centre for Nanotechnology, University College, London WC1E 6BT, UK

<sup>6</sup>College of Physics, Jilin University, Changchun, Jilin 130012, P.R. China

It has been technically challenging to concurrently probe the electrons and the lattices in materials during non-equilibrium processes, allowing their correlations to be determined. Here, in a single set of ultrafast electron diffraction patterns taken on the charge-density-wave (CDW) material 1T-TaSeTe, we discover a temporal shift in the diffraction intensity measurements as a function of scattering angle. With the help of dynamic models and theoretical calculations, we show that the ultrafast electrons probe both the valence-electron and lattice dynamic processes, resulting in the temporal shift measurements. Our results demonstrate unambiguously that the CDW is not merely a result of the periodic lattice deformation ever-present in 1T-TaSeTe but has significant electronic origin. This method demonstrates a novel approach for studying many quantum effects that arise from electron-lattice dephasing in molecules and crystals for next-generation devices.

Observation of the incoherent movements of electrons and lattice, i.e., electron-lattice dephasing in excited states is of fundamental importance to understand charge-lattice interactions [1-5]. Recently, the rapid development of ultrafast methods offers the opportunity to trace dynamics in structures for characterizing the charge-lattice interactions induced by photoexcitations [1-3, 6-12]. Many ultrafast studies have focused on CDW materials [1, 7-12] that are of great interest due to their intimate relation to a variety of captivating electronic properties including metal-insulator transition and superconductivity [4, 5, 13-15]. The symmetry-broken states of CDW are depicted by real-space charge-density re-distributions, which often result in a periodic lattice distortion (PLD) at equilibrium [16], or vice versa. It is this “electron dichotomy” reflecting distinct electronic and lattice contributions to the CDW that gives rise to much of the ongoing debates about the nature and origin of CDWs in various systems. One of the most compelling challenges in studying CDW materials is to probe the dynamics of charge states and the lattice distortions concurrently because only the co-evolution can yield the correct understanding of the driving mechanisms [1, 6, 7]. Limited by technical difficulties, however, the electron dynamics and lattice evolution in a material during non-equilibrium processes are commonly investigated by discrete methods, for instance, angle resolved photon emission spectroscopy for electron dynamics [17, 18] and x-ray diffraction for lattice dynamics [19]. Correlating the observations of the different experimental methods requires careful synchronization, however, is often an insurmountable problem due to the distinct nature of the probes and the different experimental and material conditions employed.

Electron diffraction techniques have been developed for nearly a century, with intrinsic advantages compared to other scattering tools [20] due to the high electron scattering cross-sections. Unlike for X-rays, which interact with all the electrons surrounding an atom, and are therefore sensitive to atom positions, electrons interact with the electrostatic potential of an atom - its positively charged nucleus screened by its negatively charged electron cloud [21-23]. Thus, the scattering amplitude of an atom for incident electrons at small scattering angles is determined mainly by an atom’s valence charge, rather than by the total density of electrons (see Fig.1(a)). In other words, the electron scattering atomic form factor at small scattering angles is strongly influenced by the valence electron distribution of atoms and charge transfer in a crystal. This is particularly advantageous for crystals with large unit cells that have reflections at small scattering angles [21]. In contrast, in a complementary fashion, electrons scattered to high scattering angles are extremely sensitive to subtle changes of atom positions or atomic motion.

Inspired by this feature of the scattering mechanism, we analyze the intensity of superlattice reflections (SLRs) that correspond to the CDW superstructure in the single-crystalline layered transition metal dichalcogenide 1T-TaSeTe using MeV ultrafast electron diffraction (UED) [24, 25], taking advantage of its sensitivity to the valence charge and atomic displacements, which dominate at different scattering angles. The 1T-TaSeTe single crystals were grown by chemical vapor transport with iodine as a transport agent [26]. In fact, the PLD in our samples exists at all the measureable temperatures until they melt. This raises a serious

question about whether the CDW in this material is truly of some electronic origin or merely a result of the ever-present lattice deformation. Understanding this extreme case is instrumental to resolving the aforementioned ongoing debate about the nature and origin of CDWs in various systems. The UED experiments were performed on the 3.5-MeV-UED setup at the Stanford Linear Accelerator Laboratory excited by a laser pulse with a photon energy of 1.55 eV (center wavelength of 800 nm) and a fluence of  $3.5 \text{ mJ/cm}^2$  [27]. This classic layered 1T dichalcogenide has a random Te-Se distribution on the dichalcogenide lattice site [26]; the Te/Se mixture is required to stabilize the 1T structure. The measurement temperature is 26 K to minimize the thermal atomic motion and diffuse scattering background. A portion of the UED pattern (at  $t = -2$  ps; before pumping) is shown in Fig. 1(b), with nine sets of the SLRs and their positions in reciprocal space as a function of scattering angles marked by the dashed line [28]. The subscripts 1, 2 and 3 correspond to indexes  $(hkl100)$ ,  $(hkl010)$  and  $(hkl0\bar{1}0)$ , respectively, owing to the triple-q states in the CDW [26, 27]. Normalized intensities (normalized to the averaged intensity before  $t = 0$ ) as a function of time delay from three selected SLRs are shown in Fig. 1(c). Through quantitative intensity analysis we determine the atomic positions during the lattice evolution upon photoexcitation [27]. The SLR intensities as a function of time are simulated and shown in Fig. S4 [28]. The simulation is consistent with the experiment, revealing that there is a rapid drop of the normalized intensities, which reach a minimum at a few hundred femtoseconds, then recover on a slower time scale. We use a two-exponential function to fit the SLR intensities in Fig. 1(c) which well describes the experimental observations.

Compared with the reconstructed lattice evolution using the same set of UED data [27], we notice that at the time when the SLR intensities reach the minimum (the cusp), both the Ta and Se/Te atoms depart furthest from their PLD state with distorted positions (i.e., before pumping). The temporal characteristics in the lattice evolution, particularly the time of the cusp  $t_c$ , should be equally reflected by all the SLRs suggested by the diffraction simulations of all the SLRs that  $t_c$  is the same given the same set of the atomic displacements through the dynamics (see simulated intensity variations in Fig. S4 and Fig. S5 using both kinematic and dynamic electron scattering simulations) [28]. However, unexpectedly we observe an intriguing difference in values of  $t_c$  measured for the SLRs at different scattering angles. To better visualize the shift of  $t_c$ , we renormalized the intensity plots (Fig.2(a)). The intensity renormalization affects the time constants in the two-exponential curve fitting but it does not affect the value of  $t_c$ . In Fig. 2(a), the curve fits of the intensity variations of all nine SLRs show a shift of  $t_c$  toward higher values as the scattering vector length  $s$  increases (also see inset). The measured  $t_c$  vs.  $s$  behavior is plotted in Fig. 2(b) (black dots), indicating that the value of  $t_c$  changes from  $\sim 0.48$  ps for the  $(100_1)$  reflection to  $\sim 0.88$  ps for the  $(400_1)$  reflection.

Since the evolution of atomic displacements in the lattice do not induce the measured shift in  $t_c$ , we move further to examine the lattice vibration effect on the SLRs, which are sensitive to scattering angle, on the measured  $t_c$  values. The normalized SLRs intensity at time  $t'$

can be expressed by  $\frac{I(t')}{I(t_0)} = \frac{I(u')}{I(u_0)} e^{-2B(t')s^2}$ , where  $t_0$  is time zero,  $u'$  the lattice distortion at  $t'$  and  $u_0$  the lattice distortion at  $t_0$ ,  $B(t')$  is the effective Debye-Waller (D-W) factor at  $t'$  assuming isotropic and identical for all the atoms, and  $s = \sin\theta/\lambda$  ( $\theta$  being the half of scattering angle and  $\lambda$  is the electron wavelength) as the scattering vector [20, 22]. It is widely accepted during the warm up  $B(t')$  can be expressed by  $B(t') = a(1 - e^{-t'/\tau_{DW}})$  assuming the lattice has negligible vibration at time zero, where  $\tau_{DW}$  is the time constant for the change in the lattice vibration and  $a$  describes the value of  $B(t')$  where it reaches saturation [29-31]. By applying the D-W term to the intensities of the SLRs, we find that the  $t_c$  in the intensity variation can be shifted to higher values, depending on the parameters  $a$  and  $\tau_{DW}$  in the  $B(t')$  expression. According to the intensity expression, we measured  $\frac{I(t')}{I(t_0)}$  and calculated the  $\frac{I(u')}{I(u_0)}$  for all nine SLRs at  $t' = 6$  ps when the system reaches to a quasi-stable condition. Then the parameter  $a$  is determined to be  $\sim 0.134$  ( $\text{\AA}^2$ ) by the slope of the plot of  $\ln \left[ \frac{I(t')}{I(t_0)} / \frac{I(u')}{I(u_0)} \right]$  vs.  $s^2$ , as shown in Fig. S6 [28]. While it is hard to accurately determine  $\tau_{DW}$ , we find that the D-W term has a maximum effect on the  $t_c$  value (i.e.,  $t_c$  exhibits the largest shift) when  $\tau_{DW} \sim 0.9$  ps [28]. Given all the above considerations in measurements, we remove the lattice vibration effect on the intensity variations measured from the nine SLRs by dividing the raw data by  $e^{-2B(t')s^2}$ , in which  $B(t') = 0.134(1 - e^{-t'/0.9})$ , and fit the processed data again. The corrected values of  $t_c$  are plotted as the red dots in Fig. 2(b), with the correction as scattering-angle dependent. Note that the correction for the D-W term is the upper limit of the effect in this case for the reason stated above. Therefore, the lattice behavior, including the atomic displacements and the lattice vibrations, cannot be responsible for the  $t_c$  shift that is unambiguously observed in the experiment.

To explore the origin of the  $t_c$  shift, we employ theoretical models to explain the dynamic behavior of the system. The electrons are excited abruptly by the pumping photons, and the excitation and relaxation process takes place within a few femtoseconds [6, 32, 33]. Assuming that an electronic order parameter  $\eta$  in the material relaxes in an exponential decay from the excited states, then

$$\eta(t) = \eta_f + (\eta_i - \eta_f)e^{-t/\tau_\eta}, \quad 1)$$

where  $\tau_\eta$  is the time constant for the electron relaxation, and  $\eta_i$  and  $\eta_f$  are the initial and a semi-final stage (when the measurements reach meta-stable values after  $t \sim 3$  ps [27]) of the electronic order, respectively. On the other hand, the lattice order parameter  $Q$  can be written in a dynamic equation

$$\frac{dQ}{dt} = \frac{Q - Q_f(\eta)}{\tau_Q}, \quad 2)$$

where lattice order  $Q_f$  is the final states (after 3 ps) is a function of  $\eta$  instead of a simple time-independent constant and  $\tau_Q$  describes how fast the lattice follows the change in the electronic order. Taking linear coupling between the lattice and electrons for simplicity, i.e.,  $Q_f(\eta) = \eta$ ,

Eqn. 2) is  $\frac{dQ}{dt} = \frac{Q - [\eta_f + (\eta_i - \eta_f)e^{-t/\tau_\eta}]}{\tau_Q}$ , which has an analytical solution as follows.

$$Q(t) = e^{-t/\tau_Q} + \eta_f(1 - e^{-t/\tau_Q}) + \frac{(\eta_i - \eta_f)\tau_\eta}{\tau_Q - \tau_\eta}(e^{-t/\tau_Q} - e^{-t/\tau_\eta}) \quad 3)$$

Eqn. 1) and 3) are plotted as the black and red (both bold) curves in Fig. 3 to represent the dynamics of electron and lattice, respectively, by setting  $\eta_i = 0.6$ ,  $\eta_f = 0.9$ ,  $\tau_\eta = 0.4$  and  $\tau_Q = 0.3$ . Eqn. 3) provides a phenomenological interpretation of the fitting functions that the two time-constants ( $\tau_\eta$  and  $\tau_Q$ ) are associated with the electron relaxation speed (even we measure the response of the lattice) and the speed that the lattice follows the change in electrons. The amplitudes of the two-exponential fittings, which have been often employed in UED data analysis [8, 12, 27, 34], can now be explicitly expressed by Eqn. 3). Indeed, to be comparable to the experimental results,  $\tau_\eta$  and  $\tau_Q$  need to have similar values ( $\sim 0.3$  ps in this case). This indicates that the relaxation time of the electronic order is not independent of its environment, but strongly coupled to the lattice dynamics. Such an implication is consistent with polaron-type behavior (i.e., the electron and lattice dynamics are intertwined) suggested by previous ultrafast-observations in a doped manganite [34]. Most interestingly, the theoretical plots clearly show that a mixture of the lattice order with the electronic order (see a linear combination of the black and red bold curves in Fig. 3) can explain the shift of the cusp of the curve in ultrafast-time regime. The more weight of electronic order in the mixed intensity, the faster the curve reaches its cusp. Imagining an electron beam that probes mainly the lattice dynamics with a certain portion of its diffraction intensity as being due to the electron dynamics, the intensity variation would be identical to the curves depicted in Fig. 3. In comparison to the experimental findings in Fig. 2(b) and based on the scattering principles illustrated in Fig. 1(a), we interpret the shift of measured  $t_c$  in Fig. 2(b) as arising from the co-evolution of the lattice and the electron dynamics, which are both reflected in the diffraction intensity variations. Even a few percent of electron contribution to the total intensity yields a shift of  $t_c$  for the data at small scattering vector length  $s$ , while at higher scattering angles (larger  $s$ ), the value of  $t_c$  is predominantly dictated by the lattice dynamics because the electron contribution is nearly zero.

The reflection of the electron dynamics in the UED measurements as a function of scattering vector are substantiated by density-functional-theory (DFT) calculations TaSe<sub>2</sub> in the 1T structure. The normal state, with a high-symmetry electron/lattice arrangement (no CDW), and the CDW state, with symmetry breaking, were both calculated; their charge density distributions in real-space are illustrated in Fig. 4(a). Structure factors (and intensities  $I_{total}$ ) using total charge for the nine SLRs were further derived from the calculated structures and charge density mapping for both x-ray and electron diffraction. In addition, structure factors (and

intensities  $I_{valence}$ ) using valence electrons only, that are identified to be  $5d$  and  $6s$  electrons for Ta atoms and  $4p$  electrons for Se atoms (note that other orbital electrons can also be involved in the photoexcitation), were calculated as well using the DFT results. The ratio of  $I_{valence}$  to  $I_{total}$  are plotted in Fig. 4(b) as a function of  $s$  for both x-rays and electrons. It clearly shows that both techniques manifest a scattering-angle-dependent intensity variation and the weight of valence electrons in the total intensity is much higher in electron diffraction than that in x-ray, particularly at small scattering angles. Thus the (valence) electron dynamics can well be reflected in the temporal characteristics measured from UED. Note that the DFT calculations in Fig. 4 are from  $3 \times 3$ -type CDW structures based on the experimental observations. Moreover, similar DFT calculations and the derived intensities for electron and x-ray diffractions from the Star-of-David-type (with a  $\sqrt{13} \times \sqrt{13}$  unit cell) CDW, which is the low-temperature state of 1T-TaSe<sub>2</sub>, can be found in Fig. S7 with discussions [28]. Both CDW patterns have in common that in each cluster the six nearest-neighbor Ta atoms of the central Ta atom moving towards the center. With the help of theoretical modeling and calculations, the results show that the lattice dynamics are driven by the change in the electronic structure in this material, which addresses the question of whether the origin of the superstructure originates in chemical order or electronic instability (i.e., a CDW) [4, 5, 26, 35].

Separating scattering contributions of valence electrons from a lattice of atomic nuclei and inner-shell electrons is of great importance but not a trivial task with diffraction. Because incident electrons interact with electrostatic potentials of the sample, i.e., atomic nuclei screened by the electron clouds, electron diffraction has a better capability, compared to x-ray techniques, to distinguish the contribution of valence electrons from the total scattering intensity [ref. 21, and quantitatively manifested in this work]. Our findings demonstrate a novel experimental approach to concurrently probing both lattice and electron dynamics at an ultrafast time scale because the lattice and electrons move incoherently with distinct dynamics, manifesting that 1T-TaSeTe is a bona fide CDW material in which the CDW is not merely a result of the ever-present PLD and suggesting that CDW in systems that otherwise exhibit a PLD phase transition be even more likely to have significant electronic origin.

In a broader scope, in many correlated electron systems the low-energy electrons near the Fermi level tend to self-partition into fast (itinerant) and slow (more localized) ones via various mechanisms. Well-known examples include the cuprates [38] and the iridates [39] in which the partition occurs in the momentum space as node and antinode regions, the iron-based superconductors in which the partition takes place via the orbital-selective Mott transition [40,41], and the orbital-selective Peierls transitions in CuIr<sub>2</sub>S<sub>4</sub> spinel [41] and NaTiSi<sub>2</sub>O<sub>6</sub> pyroxene [43]. Again, it is this “electron dichotomy” that gives rise to much of the ongoing debates about the nature and origin of the various unusual phenomena in those systems. As the electrons move fast or slow through the lattice, their couplings to the lattice are substantially different. Hence, the present technique is anticipated to provide novel insights into many

quantum materials by temporally separating and ultimately quantifying electron-lattice coupling on its fundamental time scales.

## Acknowledgements

Research was sponsored by DOE-BES Early Career Award Program and by DOE-BES under Contract DE-SC0012704. The work at University of Michigan was supported by NSF-EFMA-1741618. The UED experiment was performed at SLAC MeV-UED, which is supported in part by the DOE BES SUF Division Accelerator & Detector R&D program, the LCLS Facility, and SLAC under contract Nos. DE-AC02-05-CH11231 and DE-AC02-76SF00515. The work at Princeton was supported by Department of Energy, Division of Basic Energy Sciences, Grant DE-FG02-98ER45706. X.J. acknowledges the visiting scholarship of Brookhaven National Laboratory and the financial support of China Scholarship Council.

Electronic address: jtao@bnl.gov

1. Z. Tao, Tzong-Ru T. Han, Subhendra D. Mahanti, Phillip M. Duxbury, Fei Yuan, Chong-Yu Ruan, Kevin Wang, and Junqiao Wu, *Phys. Rev. Lett.* **109**, 166406 (2012).
2. K. Ishioka, M. Hase, & M. Kitajima, *Phys. Rev. B* **77**, 121402 (2008).
3. Mark J. Stern, Laurent P. René de Cotret, Martin R. Otto, Robert P. Chatelain, Jean-Philippe Boisvert, Mark Sutton, and Bradley J. Siwick, *Phys. Rev. B* **97**, 165416 (2018).
4. K. Rossnagel, *J. Phys.: Condens. Matter* **23**, 213001 (2011).
5. X. Zhu, Y. Cao, J. Zhang, E. W. Plummer & J. Guo, *Proc. Natl. Acad. Sci. USA* **112**, 2367-2371 (2015).
6. T. Konstantinova, Jonathan D. Rameau, Alexander H. Reid, Omadillo Abdurazakov, Lijun Wu, Renkai Li, Xiaozhe Shen, Genda Gu, Yuan Huang, Laurenz Rettig, Isabella Avigo, Manuel Ligges, James K. Freericks, Alexander F. Kemper, Hermann A. Dürr, Uwe Bovensiepen, Peter D. Johnson, Xijie Wang and Yimei Zhu, *Sci. Adv.* **4**, eaap7427 (2018).
7. Martin R. Otto, Laurent P. René de Cotret, David A. Valverde-Chavez, Kunal L. Tiwari, Nicolas Émond, Mohamed Chaker, David G. Cooke, and Bradley J. Siwick, *PNAS* **116**, 450 (2019)
8. Maximilian Eichberger, Hanjo Schafer, Marina Krumova, Markus Beyer, Jure Demsar, Helmuth Berger, Gustavo Moriena, German Sciaini & R. J. Dwayne Miller, *Nature* **468**, 799-802 (2010).
9. Tzong-Ru T. Han, Faran Zhou, Christos D. Malliakas, Phillip M. Duxbury, Subhendra D. Mahanti, Mercouri G. Kanatzidis and Chong-Yu Ruan, *Sci. Adv.* **1**, e1400173 (2015).
10. Alfred Zong, Xiaozhe Shen, Anshul Kogar, Linda Ye, Carolyn Marks, Debanjan Chowdhury, Timm Rohwer, Byron Freelon, Stephen Weathersby, Renkai Li, Jie Yang, Joseph Checkelsky, Xijie Wang and Nuh Gedik. *Sci. Adv.* **4**, eaau5501 (2018).

11. Simon Wall, Shan Yang, Luciana Vidas, Matthieu Chollet, James M. Glowonia, Michael Kozina, Tetsuo Katayama, Thomas Henighan, Mason Jiang, Timothy A. Miller, David A. Reis, Lynn A. Boatner, Olivier Delaire, Mariano Trigo, *Science* **362**, 525-526 (2018).
12. Alfred Zong, Anshul Kogar, Ya-Qing Bie, Timm Rohwer, Changmin Lee, Edoardo Baldini, Emre Ergecen, Mehmet B. Yilmaz, Byron Freelon, Edbert J. Sie, Hengyun Zhou, Joshua Straquadine, Philip Walmsley, Pavel E. Dolgirev, Alexander V. Rozhkov, Ian R. Fisher, Pablo Jarillo-Herrero, Boris V. Fine and Nuh Gedik. *Nat. Phys.* **15**, 27-31 (2019).
13. J. A. Wilson & A. D. Yoffe, *Adv. Phys.* **18**, 193-335 (1969).
14. Pollak, R. A., Eastman, D. E., Himpfel, F. J., Heimann, P. & Reihl, B. *Phys. Rev. B* **24**, 7435-7438 (1981).
15. J. Chang, E. Blackburn, A. T. Holmes, N. B. Christensen, J. Larsen, J. Mesot, Ruixing Liang, D. A. Bonn, W. N. Hardy, A. Watenphul, M. v. Zimmermann, E. M. Forgan & S. M. Hayden, *Nature Phys.* **8**, 871-876 (2012).
16. J. A. Wilson, F. J. Di Salvo & S. Mahajan, *Adv. Phys.* **24**, 117-201 (1975).
17. C. L. Smallwood, R. A. Kaindl & A. Lanzara, *Europhys. Lett.* **115**, 27001 (2016).
18. S. Gerber, S.-L. Yang, D. Zhu, H. Soifer, J. A. Sobota, S. Rebec, J. J. Lee, T. Jia, B. Moritz, C. Jia, A. Gauthier, Y. Li, D. Leuenberger, Y. Zhang, L. Chaix, W. Li, H. Jang, J.-S. Lee, M. Yi, G. L. Dakovski, S. Song, J. M. Glowonia, S. Nelson, K. W. Kim, Y.-D. Chuang, Z. Hussain, R. G. Moore, T. P. Devereaux, W.-S. Lee, P. S. Kirchmann, Z.-X. Shen, *Science* **357**, 71 (2017).
19. K. J. Gaffney & H. N. Chapman, *Science* **316**, 1444-1448 (2007).
20. J. M. Zuo & J. C. H. Spence, *Advanced transmission electron microscopy* (Springer, New York, 2017).
21. J.-C. Zheng, Y. Zhu, L. Wu & J. W. Davenport, *J. Appl. Cryst.* **38**, 648-656 (2005).
22. L.-M. Peng, *Micron* **30**, 625-648 (1999).
23. M. Stefanou, K. Saita, D. V. Shalashilin & A. Kirrander, *Chem. Phys. Lett.* **683**, 300-305 (2017).
24. X. J. Wang, Z. Wu, & H. Ihee, *Proc. 2003 Part Accel. Conf.* **1**, 420-422 (2003).
25. S. P. Weathersby, G. Brown, M. Centurion, T. F. Chase, R. Coffee, J. Corbett, J. P. Eichner, J. C. Frisch, A. R. Fry, M. Gühr, N. Hartmann, C. Hast, R. Hettel, R. K. Jobe, E. N. Jongewaard, J. R. Lewandowski, R. K. Li, A. M. Lindenberg, I. Makasyuk, J. E. May, D. McCormick, M. N. Nguyen, A. H. Reid, X. Shen, K. Sokolowski-Tinten, T. Vecchione, S. L. Vetter, J. Wu, J. Yang, H. A. Dürr, and X. J. Wang, *Rev. Sci. Instrum.* **86**, 73702 (2015).
26. Huixia Luo, Weiwei Xie, Jing Tao, Hiroyuki Inoue, András Gyenis, Jason W. Krizan, Ali Yazdani, Yimei Zhu, and Robert Joseph Cava, *Proc. Natl. Acad. Sci. USA* **112**, E1174-E1180 (2015).
27. Jun Li, Junjie Li, Kai Sun, Lijun Wu, Haoyun Huang, Renkai Li, Jie Yang, Xiaozhe Shen, Xijie Wang, Huixia Luo, Robert J. Cava, Ian K. Robinson, Yimei Zhu, Weiguo Yin, Jing Tao, <http://arxiv.org/abs/1903.09911>

28. See Supplemental Material at [URL will be inserted by publisher] for details in UED data analysis and D-W correction methods with ref. 36 and 37.
29. Linlin Wei, Shuaishuai Sun, Cong Guo, Zhongwen Li, Kai Sun, Yu Liu, Wenjian Lu, Yuping Sun, Huanfang Tian, Huaixin Yang, and Jianqi Li, *Struct. Dyn.* **4**, 044012 (2017).
30. F. Carbone, D. S. Yang, E. Giannini & A. H. Zewail, *Proc. Natl. Acad. Sci. USA* **105**, 20161 (2008).
31. M. Harb, H. Enquist, A. Jurgilaitis, F. T. Tuyakova, A. N. Obraztsov, and J. Larsson, *Phys. Rev. B* **93**, 104104 (2016).
32. Zhensheng Tao, Cong Chen, Tibor Szilvási, Mark Keller, Manos Mavrikakis, Henry Kapteyn, Margaret Murnane, *Science* **353**, 62-67 (2016).
33. Chen, J. K., Tzou, D. Y. & Beraun, J. E. A semiclassical two-temperature model for ultrafast laser heating. *Int. J. Heat Mass Tran.* **49**, 307-316 (2006).
34. Junjie Li, Wei-Guo Yin, Lijun Wu, Pengfei Zhu, Tatianna Konstantinova, Jing Tao, Junjie Yang, Sang-Wook Cheong, Fabrizio Carbone, James A Misewich, John P Hill, Xijie Wang, Robert J Cava and Yimei Zhu, *NPJ Quant. Mater.* **1**, 16026 (2016).
35. Y. Liu, D. F. Shao, L. J. Li, W. J. Lu, X. D. Zhu, P. Tong, R. C. Xiao, L. S. Ling, C. Y. Xi, L. Pi, H. F. Tian, H. X. Yang, J. Q. Li, W. H. Song, X. B. Zhu, and Y. P. Sun, *Phys. Rev. B* **94**, 045131 (2016).
36. Pengfei Zhu, Y Zhu, Y Hidaka, L Wu, J Cao, H Berger, J Geck, R Kraus, S Pjetrov, Y Shen, *New J. Phys.* **17**, 063004 (2015).
37. P. A. Midgley, & A. S. Eggeman, *IUCrJ* **2**, 126-136 (2015).
38. M. R. Norman, H. Ding, M. Randeria, J. C. Campuzano, T. Yokoya, T. Takeuchi, T. Takahashi, T. Mochiku, K. Kadowaki, P. Guptasarma, D. G. Hinks, *Nature* **392**, 157 (1998).
39. Y. K. Kim, O. Krupin, J. D. Denlinger, A. Bostwick, E. Rotenberg, Q. Zhao, J. F. Mitchell, J. W. Allen, B. J. Kim, *Science* **345**, 187 (2014).
40. Luca de' Medici, S. R. Hassan, Massimo Capone, and Xi Dai, *Phys. Rev. Lett.* **102**, 126401 (2009).
41. W.-G. Yin, C.-C. Lee, and W. Ku, *Phys. Rev. Lett.* **105**, 107004 (2010).
42. E.S. Bozin, W.G. Yin, R.J. Koch, M. Abeykoon, Y.S. Hor, H. Zheng, H.C. Lei, C. Petrovic, J.F. Mitchell & S.J.L. Billinge, *Nat. Commun.* **10**:3638 (2019).
43. A. Feiguin, A. M. Tsvelik, Weiguo Yin, E. S. Bozin, *Phys. Rev. Lett.* **123**, 237204 (2019).

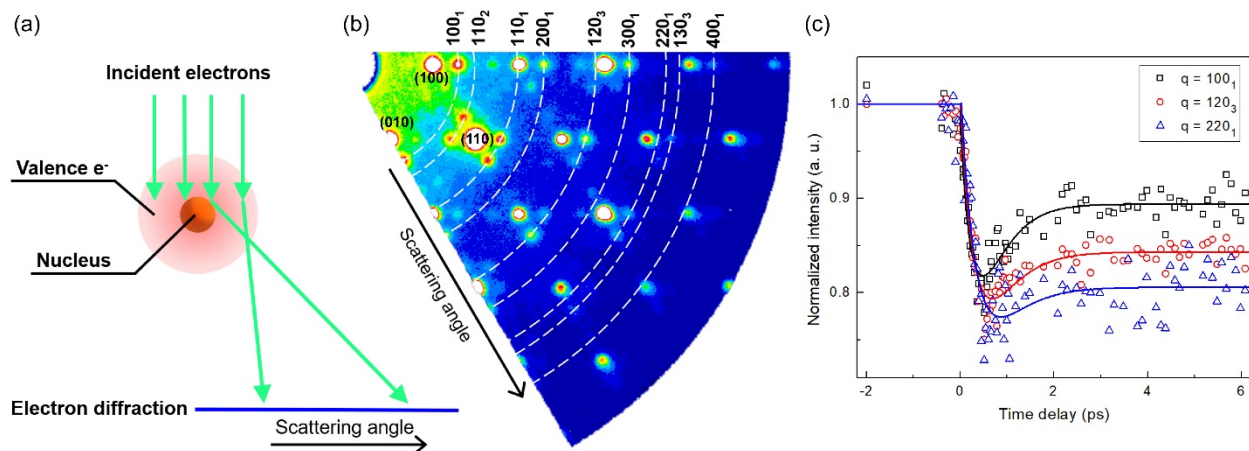


Figure 1. Scattering-angle-dependent dynamics measured via ultrafast electron diffraction (UED). (a) A schematic representation of electron scattering, illustrating that scattering from valence electrons is predominant at small scattering angles, while it is from nuclei at high scattering angles. (b) A part of an experimental UED pattern showing multiple Bragg reflections and superlattice reflections (SLRs). Nine sets of SLRs were selected for the measurements with their scattering angles marked by the dashed lines. (c) Intensity variation (normalized by the averaged intensity before pumping) vs. time delay measured from representative SLRs. The solid lines are fittings of the experimental data to a two-exponential model.

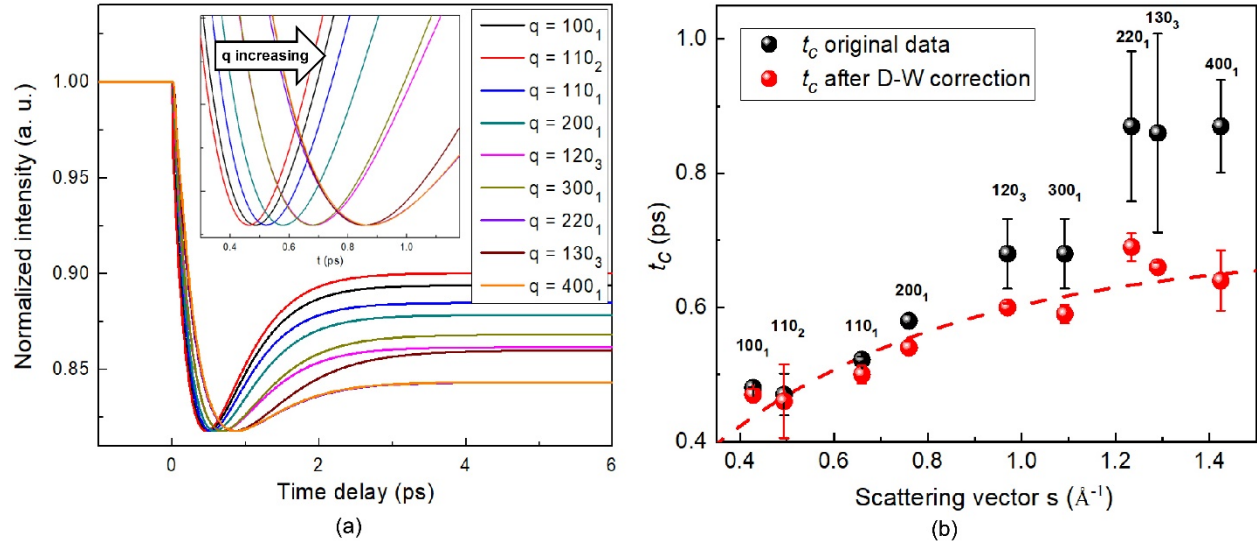


Figure 2. Measurement of the time at the cusp point  $t_c$  of the SLRs during the lattice relaxation process as a function of the scattering vector length  $s$ . (a) Two-exponential fitting curves for nine sets of SLRs, showing a shift of  $t_c$  toward increased time delay with the increase of scattering vector  $s$ . (b) A plot of  $t_c$  vs. the scattering vector length  $s$  of the SLRs. The black dots are measured directly from the fitting of the raw diffraction data. The red dots are the measurements after the removal of the influence of the Debye-Waller (D-W) factors on the values of  $t_c$  [28]. The red dashed line is a guide to the eye for the red dots. The error bars mean the deviation of the  $t_c$  values determined in two distinct fitting methods, as shown in Fig. S2, S2-1 and S2-2 [28].

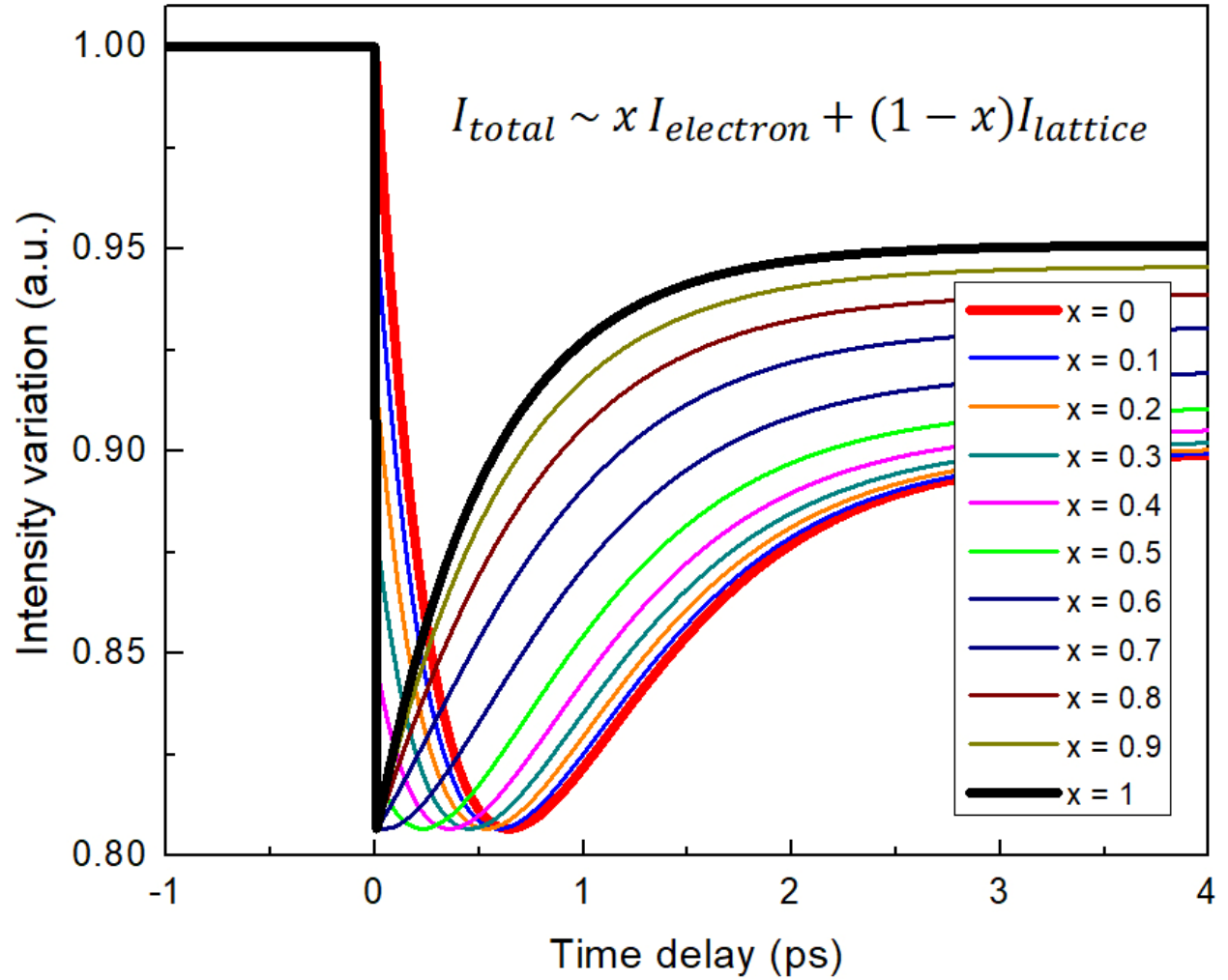


Figure 3. Intensity variation as a function of time derived from dynamic models. The bold black curve reflects the electron while the bold red curve reflects the lattice dynamics considering the electron relaxation rate and the electron-lattice coupling time constant. Colored curves are the linear combinations of the black and the red curves, indicating a shift of  $t_c$  as a function of  $x$ , or the weight of the electron dynamics, in the total measurement.

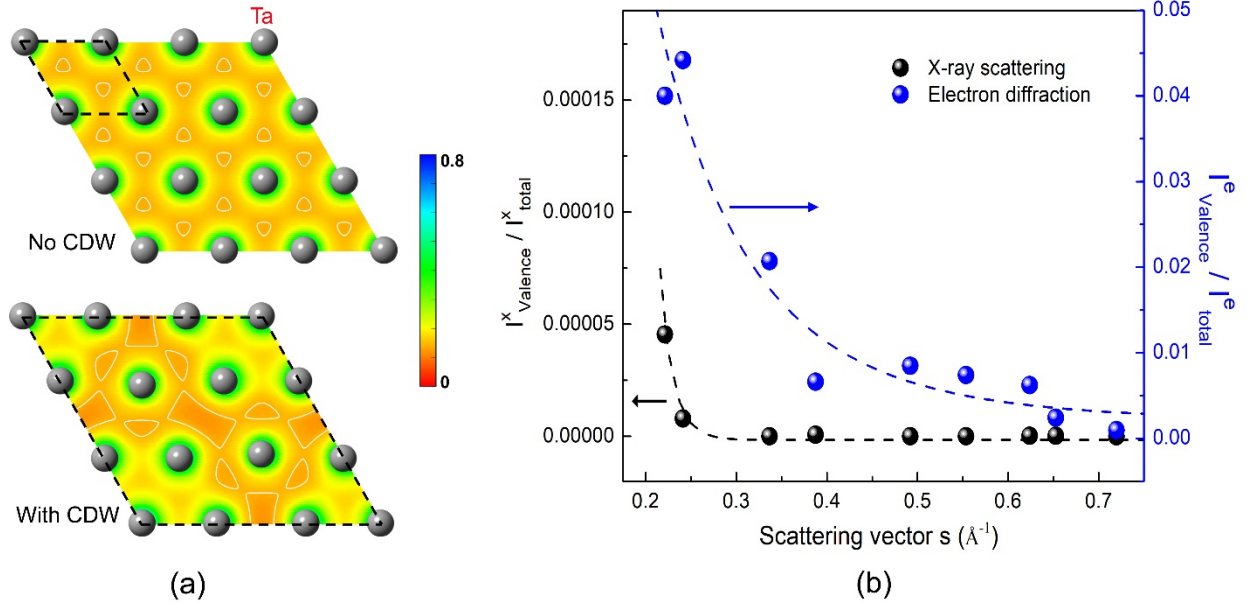


Figure 4. Calculated (planar) charge density distributions and associated x-ray/electron scattering intensities. (a) Charge density mapping of the Ta plane (Ta atoms are shown) in 1T-TaSe<sub>2</sub> based on DFT calculations for the state with no CDW (upper; unit cell marked by the black dashed lines) and the CDW state (lower; unit cell is 3×3 times larger). The color scale shows the number of electrons in unit-cell volume. (b) Structure factors of the CDW state were calculated, corresponding to the nine measured SLRs, using valence charges (5*d* and 6*s* electrons for Ta atoms and 4*p* electrons for Se atoms) and total charges of Ta and Se atoms based on the electronic structures in (a). The ratios of the scattering intensity from valence electrons to the total intensity are obtained and plotted for x-ray (black dots) and electron diffraction (blue dots). Note that the scales are different for x-ray and electron scattering. The dashed lines are guides to the eye.